Fusion protein EWS-FLI1 is incorporated into a protein granule in cells

Nasiha S. Ahmed[1], Lucas M. Harrell[2], Jacob Schwartz[2]*

[1] Department of Molecular and Cellular Biology, The University of Arizona, Tucson, AZ 85719

[2] Department of Chemistry and Biochemistry, The University of Arizona, Tucson, AZ 85719

* Corresponding author: jcschwartz@email.arizona.edu

Keywords: Ewing sarcoma, fusion proteins, phase separation, granules, transcription

ABSTRACT

Ewing sarcoma is driven by fusion proteins containing a low complexity (LC) domain that is intrinsically disordered and a powerful transcriptional regulator. The most common fusion protein found in Ewing sarcoma, EWS-FLI1, takes its LC domain from the RNA-binding protein EWSR1 (Ewing Sarcoma RNA-binding protein 1) and a DNA-binding domain from the transcription factor FLI1 (Friend Leukemia Virus Integration 1). The LC domain in EWS-FLI1 can bind RNA polymerase II (RNA Pol II) and can self-assemble through a process known as phase separation. The ability of EWSR1 and related RNA-binding proteins to assemble into ribonucleoprotein granules in cells has been intensely studied but the role of phase separation in EWS-FLI1 activity is less understood. We investigated the overlapping functions of EWSR1 and EWS-FLI1 in controlling gene expression and tumorigenic cell growth in Ewing sarcoma, and our results suggested that these proteins function closely together. We then studied the nature of interactions among EWS-FLI1, EWSR1, and RNA Pol II. We observed EWSR1 and RNA Pol II to be present in protein granules in cells. We then identified protein granules in cells associated with the fusion protein, EWS-FLI1. The tyrosine residues in the LC domain are required for the abilities of EWS-FLI1 to bind its partners, EWSR1 and RNA Pol II, and to incorporate into protein granules. These data suggest that interactions among EWS-FLI1, RNA Pol II, and EWSR1 in Ewing sarcoma can occur in the context of a molecular scaffold found within protein granules in the cell.

INTRODUCTION

RNA-binding proteins are key players in every step of mRNA biogenesis (Moore and Proudfoot 2009). The FET proteins are a family of highly homologous and ubiquitously expressed RNA-binding proteins comprising FUS, EWSR1, and TAF15. These proteins are predominantly nuclear and bind thousands of RNA with degenerate specificity (Schwartz et al. 2015; Ozdilek et al. 2017). Although significantly more published work has focused on the activities of FUS in cells, recent studies have begun to shed light on the properties and functions of EWSR1. A number of cellular functions of the FET proteins overlap, such as the regulation of expression from thousands of genes (Luo et al. 2015; Masuda et al. 2015; Schwartz et al. 2012; Hoell et al. 2011). FUS and EWSR1 each bind the C-terminal domain (CTD) of RNA Pol II and modulate its phosphorylation (Kwon et al. 2013; Schwartz et al. 2013; Gorthi et al. 2018). EWSR1 has also been shown to bind nascent RNA transcripts, a number of RNA processing factors, and transcription factors (Chi et al. 2018). This extensive network of interactions maintained by FET proteins provide them several avenues that broadly affect gene expression (Paronetto et al. 2011; Rogelj et al. 2012; Masuda et al. 2015).

The FET protein genes are frequently involved in genomic translocation events in sarcomas (Riggi et al. 2007; Tan and Manley 2009). The second most common pediatric bone cancer is Ewing sarcoma. These tumors result from a translocation event that fuses the N-terminal low complexity (LC) domain of a FET protein and the DNA-binding domain (DBD) of an ETS transcription factor. For 85% of Ewing sarcomas, the LC domain of EWSR1 and the DBD from the FLI1 combine to form the oncogenic protein EWS-FLI1 (Delattre et al. 1992; Grünewald et al. 2018). Ewing sarcoma is generally considered to arise from mesenchymal stem cells (Riggi et al. 2005, 2008). Expression of EWS-FLI1 is sufficient for transformation in Ewing sarcoma (Kovar et al. 1996; Tanaka et al. 1997). The FLI1 DBD in EWS-FLI1 recognizes a short DNA sequence GGAA and functions most efficiently for enhancer regions containing 10 or more repeats of the motif (Gangwal et al. 2008; Bailly et al. 1994). Like the wild-type FET proteins, EWS-FLI1 binds RNA Pol II, as well as a number of transcription factors and enhancer or repressor complexes (Sankar et al. 2013; Riggi et al. 2014; Boulay et al. 2017; Selvanathan et al. 2019). Nevertheless, the mechanism for EWS-FLI1 to broadly modulate transcription remains incompletely understood.

A striking property of FET proteins is their ability to assemble into higher-order ribonucleoprotein (RNP) assemblies in a process known as phase separation (Kato et al. 2012; Kwon et al. 2013). RNA seeds this assembly

process and it is the oligomerized protein that binds RNA Pol II (Kwon et al. 2013; Schwartz et al. 2013). The LC domains of FET proteins contain a number of repeated [S/G]Y[S/G] motifs. The tyrosine residues contained in this motif are critical for the domain to undergo phase separation (Kwon et al. 2013; Kato et al. 2012; Boulay et al. 2017). In cells, phase separation gives rise to several RNP granules, including stress granules and processing (P)–bodies in the cytoplasm and nucleoli in the nucleus. Several recent studies have provided evidence that phase separation modulates transcription (Boeynaems et al. 2018). FET proteins would naturally be predicted to be involved in this form of transcription control (Jain et al. 2016; West et al. 2016; Blechingberg et al. 2012).

The LC domain contained in EWS-FLI1 transfers the ability to phase separate to the fusion protein (Chong et al. 2018; Boulay et al. 2017). EWS-FLI1 binds and recruits EWSR1 to enhancer regions and assemblies formed by an EWSR1 fusion protein interact with RNA Pol II (Spahn et al. 2003; Embree et al. 2009; Boulay et al. 2017). Interestingly, the homotypic self-interactions of the LC domain are required to stabilize EWS-FLI1 binding at GGAA microsatellites in cells. Phase separation by EWS-FLI1 along chromosomal DNA is also required for the fusion protein to control transcription and initiate transformation. Our lab has shown that FUS and RNA Pol II interact with each other in a nuclear granule (Thompson et al. 2018; Schwartz et al. 2012). The role that phase separation plays in the functions of FET-fusion proteins suggests that they may also incorporate into protein granules in cells.

We investigated the ability of EWS-FLI1 to associate with protein granules in cells. We first extended the body of evidence to confirm that EWSR1 cooperates with EWS-FLI1 to modify gene expression and cell transformation. Subsequently, we applied crosslinking-based methods to explore whether EWSR1 and EWS-FLI1 occupy large protein particles in cells. The aim of this study was to augment understanding of the role of EWS-FLI1 in transcription and transformation by characterizing the properties of the assemblies that the protein forms in cells.

RESULTS

Transcript levels in Ewing sarcoma are affected by both EWSR1 and EWS-FLI1

EWSR1 and EWS-FLI1 share the same LC domain, which undergoes oligomerization for the proteins to regulate transcription (Kwon et al. 2013; Kato et al. 2012; Boulay et al. 2017). Previous studies have demonstrated that homotypic self-interactions by the EWS-FLI1 LC domain are required to affect transcription and transformation

(Kwon et al. 2013; Chong et al. 2018; Johnson et al. 2017). Additionally, EWS-FLI1 recruits EWSR1 to GGAA-rich sites along chromosomal DNA (Gorthi et al. 2018; Boulay et al. 2017). The interaction of the fusion and wildtype LC domain proteins may contribute to their activity in Ewing sarcoma.

We used RNA-seq to determine how many genes were regulated by both EWSR1 and EWS-FLI1. We quantified abundances for poly-adenylated RNA transcripts in an Ewing sarcoma cell line, A673, which expresses *EWS-FLI1* and *EWSR1*. We knocked down expression of EWS-FLI1, EWSR1, or both using small interfering RNA (siRNA). Each siRNA was selected following a screen of 6 siRNA sequences (**Figure 1A**, *top*). The siRNA specific for EWS-FLI1 (siEF) targeted the 3´ region of EWS-FLI1 mRNA, which reduced EWS-FLI1 protein by 60% compared with a control (siSCR) by western blot (**Figure 1A**, *bottom*). The siRNA specific for EWSR1 (siEWSR1) reduced EWSR1 protein by 80% compared with siSCR. The siRNA knocking down both proteins (siE-EF) targeted the 5´ region of both mRNAs and reduced levels of each protein by 80%. We did not observe non-specific changes in EWSR1 or EWS-FLI1 protein levels by siEF or siEWSR1, respectively (**Supplemental Figure S1A**).

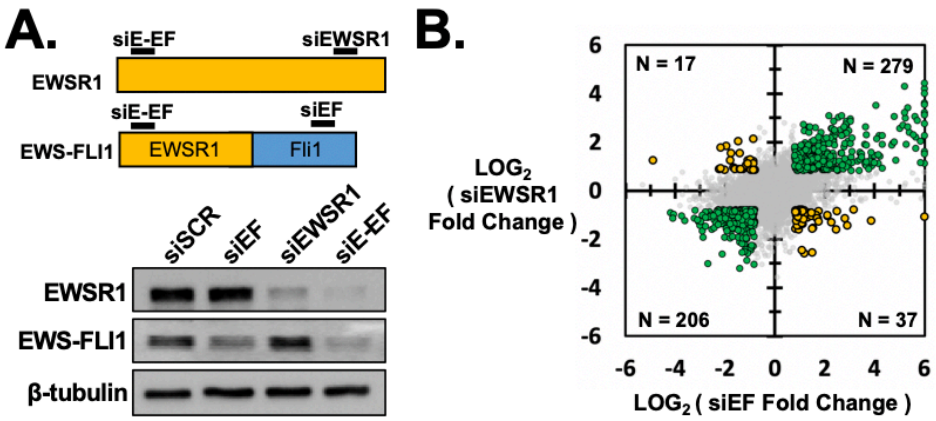

Figure 1. A large number of transcripts had similar responses after a loss of EWS-FLI1 or EWSR1 in Ewing sarcoma. (**A**) Schematic (*top*) shows locations in *EWSR1* or *EWS-FLI1* mRNA targeted by siRNA. Western blots show the reduction in protein levels in A673 cells treated with siRNA targeting EWS-FLI1 (siEF), EWSR1 (siEWSR1) or both (siE-EF). (**B**) A comparison of cells treated with siEF or siEWSR1 revealed a similar increase or decrease in abundance by >1.8-fold for 485 transcripts (green) and in the opposite directions for 54 transcripts (yellow). The number of transcripts changed >1.8-fold are indicated in each quartile.

By RNA-seq analysis, we assessed changes in transcript abundance for the top 6932 transcripts expressed in all four treatments. A large fraction of gene transcripts (n = 2026) were increased or decreased in abundance by >1.8-fold following EWS-FLI1 knockdown from siEF. Of those transcripts affected by siEF, 43% were increased in abundance (n = 875) and the remaining decreased (n = 1151). Fewer transcripts changed in abundance following EWSR1 knockdown by siEWSR1 (n = 1073). Of those, a similar 43% saw increased abundance (n = 459) and the remainder were decreased (n = 614). A substantial number of transcripts were similarly affected by the knockdown of either EWS-FLI1 or EWSR1 (n = 485, **Supplemental Figure S1B**). The knockdown of either protein resulted in an increase for 58% of these transcripts (n = 279) and a decrease for the 43% remaining (n = 206) (**Figure 1B**, shown in green). We noted that only 54 transcripts were altered in opposing directions for EWS-FLI1 and EWSR1 knockdown (**Figure 1B**, shown in gold).

We compared changes in RNA transcript levels for the loss of the individual proteins with those for the simultaneous loss of EWS-FLI1 and EWSR1. For genes whose transcript abundance responded to the loss of either protein, most (86%, or n = 418) were also changed by a simultaneous knockdown of both. Nearly all genes had the same positive or negative direction for their changes, except for 33 genes whose direction opposed that of the individual knockdowns (**Supplemental Figure S1C**). Taken together, nearly a quarter of gene transcripts controlled by EWS-FLI1 were shown to be under the control of EWSR1. Conversely, nearly half of the gene transcripts responding to the loss of EWSR1 were found to be under the control of EWS-FLI1. This finding agreed with the hypothesis that EWSR1 and EWS-FLI1 may affect expression of many of the same gene targets.

EWSR1 is required for anchorage-independent growth in Ewing sarcoma.

The loss of EWS-FLI1 is known to block anchorage-independent cell growth for Ewing sarcoma cell lines, as seen by the soft agar colony formation assay (Smith et al. 2006; Chaturvedi et al. 2012). We tested whether this tumorigenic capacity was also influenced by the EWSR1 protein. If EWS-FLI1 and EWSR1 interactions were functional and significant for Ewing sarcoma biology, a loss of either protein would be expected to result in a similar effect on this important marker of cell transformation.

We quantified growth by cell count for A673 cells after EWSR1 or EWS-FLI1 knockdown. These measurements indicated no change in growth up to 96 hours after transfection, compared with siSCR control

(**Supplemental Figure S2A**). Twenty-four hours after siRNA transfection, cells were seeded on soft agar and grown for 3 to 4 weeks. Quantifying the number of colonies formed revealed that the loss of EWS-FLI1 resulted in 60% fewer colonies compared with siSCR transfection, as had been previously reported (n = 3, $p = 0.04$, Student's t-test, **Figure 2A** and **2B**) (Chong et al. 2018; Johnson et al. 2017). Cells with EWSR1 knocked down by siEWSR1 also produced 90% fewer colonies, revealing an EWSR1 dependency for growth on a soft agar substrate (n = 3, $p = 0.004$, Student's *t*-test). We applied the soft agar assay to a second Ewing sarcoma cell line, SK-N-MC, which also expresses EWS-FLI1. Using western blot, knockdown by siEF and siEWSR1 was comparable between SK-N-MC and A673 cells (**Supplemental Figure S2B**). Knockdown produced 80% fewer colonies on soft agar in the SK-N-MC cell line for EWS-FLI1 and 90% fewer colonies for EWSR1 knockdown (**Supplemental Figure S2C and S2D**).

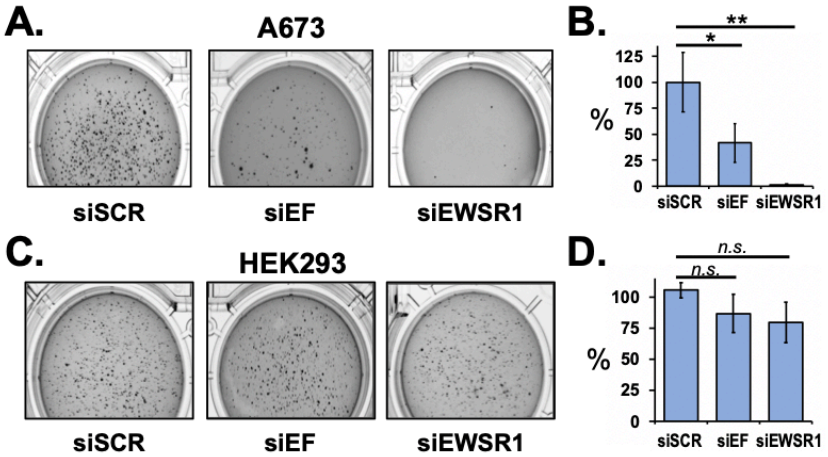

Figure 2. Loss of EWSR1 inhibits anchorage-independent growth in Ewing sarcoma cells. (**A**) Soft agar assays were performed for A673 cells treated with siSCR, siEF, or siEWSR1. (**B**) Averaged colony numbers in A673 cells were quantified relative to siSCR treatments (n = 3). (**C**) Soft agar assays were performed for HEK293T/17 cells treated with siSCR, siEF, or siEWSR1. (**D**) Averaged colony numbers for HEK293T/17 cells were quantified relative to siSCR treatments (n = 4). Error bars represent standard deviation about the mean. Student's *t*-test was calculated assuming equal variances: ** $p < 0.01$; * $p < 0.05$; n.s., not significant ($p > 0.05$).

We next asked whether EWSR1 was required for growth on soft agar in a cell line lacking the EWS-FLI1 fusion protein. We chose HEK293T/17 cells, which also does not express detectable levels of FLI1 protein. Transfection

with siEWSR1 effectively diminished EWSR1 protein but transfection with siEF had no effect (**Supplemental Figure S2E**). HEK293T/17 cells treated with siEWSR1, siEF, or the siSCR control produced similar colony numbers on soft agar (n = 4, $p > 0.05$, Student's *t*-test, **Figure 2C** and **2D**). This result raised the possibility that the role of EWSR1 may be modified by EWS-FLI1 in the cell.

Noting that the EWSR1 knockdown did not produce an effect on HEK293T/17 growth on soft agar, we asked whether introducing the fusion protein would reproduce the result observed in Ewing sarcoma cells. We expressed V5-tagged EWS-FLI1 protein in HEK293T/17 cells (**Supplemental Figure S3A**). HEK293T/17 cells expressing the fusion protein produced 60% fewer colonies after the loss of EWSR1 and compared with the siSCR-treated control (n = 6, $p < 0.001$, Student's *t*-test, **Figure 3A** and **3B**). We considered whether the effects of EWS-FLI1 on EWSR1 involved a direct interaction between the proteins in HEK293T/17 cells(Chong et al. 2018; Gorthi et al. 2018; Boulay et al. 2017). Using immunoprecipitation (IP) with antibodies that bind EWSR1 and not the fusion protein, western blot assays indicated EWS-FLI1 protein eluted with EWSR1 but not the non-specific IgG control IP (**Supplemental Figure S3B**). These experiments confirmed the presence of a physical interaction between EWS-FLI1 and EWSR1 in the HEK293T/17 cells that were changed to become sensitive to the loss of EWSR1.

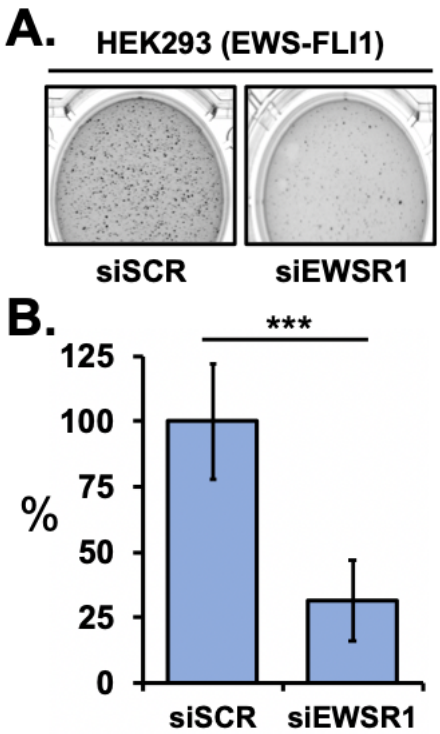

Figure 3. Expression of EWS-FLI1 in HEK293T/17 cells recapitulates loss of EWSR1 phenotype. (**A**) Soft agar assays were used to assess anchorage-independent growth of HEK293T/17 cells co-transfected with V5-EWS-FLI1 and either siEWSR1 or siSCR (n = 6). (**B**) The average reduction in colony number for siEWSR1-treated cells was quantified relative to that of siSCR. Error bars represent standard deviation about the mean. Student's *t*-test was calculated for assuming equal variances: *** $p < 0.001$.

EWSR1 and RNA Pol II associate with protein granules in cells

The LC domain shared by FET proteins and fusion proteins driving Ewing sarcoma are capable of undergoing phase separation, which is tied to the formation of granule bodies in cells (Kato et al. 2012; Kato and McKnight 2018; Lin et al. 2015). All three FET proteins bind RNA Pol II to regulate transcription (Yang et al. 2000; Kwon et al. 2013; Schwartz et al. 2012). We previously reported a granular body comprising FUS and RNA Pol II(Thompson et al. 2018). Consistent with the weak interactions found for products of phase separation *in vitro*, granules could not survive lysis unless stabilized by formaldehyde crosslinking(Wang et al. 2018; Qamar et al. 2018). Now we tested whether EWSR1 was also found in a granule in cells.

We used a separation-based approach and HEK293T/17 cells to characterize the size of protein particles containing EWSR1 and RNA Pol II, with or without formaldehyde crosslinking(Thompson et al. 2018). Nucleic acids were depleted by sonication and nuclease treatment before lysates were passed through size-exclusion chromatography (SEC) using a CL-2B column, which can separate particles up to 250 nm in diameter. UV absorption indicated most cellular proteins were present in fractions eluting after 20 mL, which was expected for monomers and complexes less than 20 nm in diameter (n = 3, **Supplemental Figure S4A**). UV absorption indicated that formaldehyde crosslinking did not appreciably change the elution of most cellular proteins, indicating most proteins were not in large particles or granules that could be stabilized by formaldehyde crosslinking (n = 3, **Figure 4A**, top).

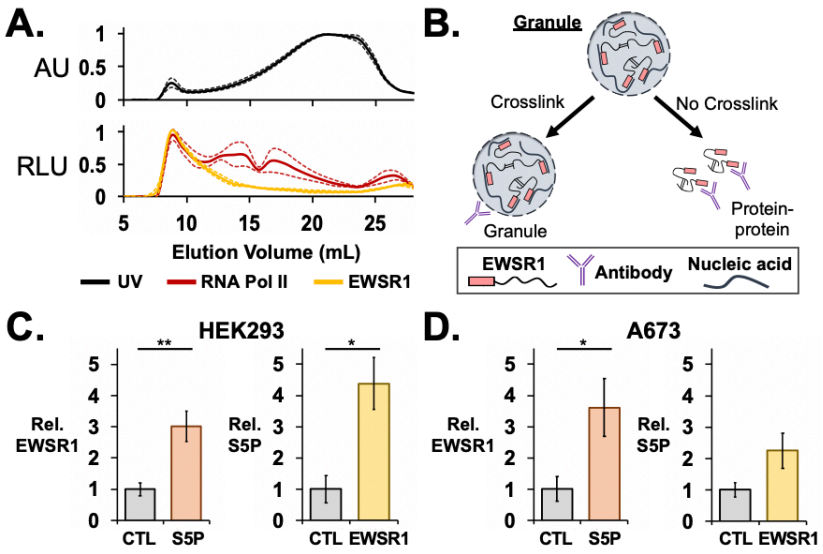

Figure 4. EWSR1 and RNA Pol II are assembled in large protein granules. (**A**) Protein eluting from size-exclusion chromatography (SEC) of HEK293T/17 cell lysates was assessed by UV absorbance (top). ELISAs were used to measure RNA Pol II and EWSR1 elution from SEC (n = 3). Dashed lines represent standard error. (**B**) The diagram compares protocols for immunoprecipitation (IP) from cells. Non-crosslinked IP assays preferentially enrich macromolecular complexes. Crosslinked IP assays are capable of recovering weak protein interactions in cell granules. Assays performed used antibodies specific for EWSR1 or CTD phosphorylated at position Ser5 (S5P). (**C**) ELISAs detected EWSR1 eluted from crosslinked IP assays of S5P in HEK293T/17 cells, and S5P was detected for crosslinked IP of EWSR1 (n = 3). (**D**) In crosslinked IP assays from A673 cells, ELISAs also detected EWSR1 eluted with S5P, and S5P was detected for crosslinked IP of EWSR1 (n = 3). AU = absorbance units. RLU = relative luminescence units. Student's *t*-test was calculated assuming equal variances: ** $p < 0.01$; * $p < 0.05$; n.s., not significant ($p > 0.05$).

SEC fractions were probed for RNA Pol II and EWSR1 by ELISA, because formaldehyde crosslinking interferes with the SDS-PAGE step for western assays. The largest diameter of the RNA Pol II holoenzyme is 25 nm and we found its elution in un-crosslinked cells to be maximal near the expected volume of 18 to 20 mL (**Supplemental Figure S4B**). EWSR1 eluted at >20 mL, indicating smaller protein particles or monomers. Formaldehyde crosslinking resulted in RNA Pol II eluting at volumes <15 mL, which indicates particles of 50 to >150 nm in diameter (**Figure 4A**). Most EWSR1 protein was detected to elute in large particles.

We tested whether EWSR1 and RNA Pol II were crosslinked together in HEK293T/17 cells. RNA Pol II was immunoprecipitated using an antibody specific for the Serine-5 phosphorylated (S5P) form. Significant enrichment for EWSR1 eluting with the polymerase was observed in ELISA assays, relative to a protein G bead control (n = 3, $p = 0.009$, Student's *t*-test, **Figure 4C**, left). By IP for EWSR1, we also found enrichment for S5P RNA Pol II (n = 3, $p = 0.02$, Student's *t*-test, **Figure 4C**, right). We repeated the IP assay for crosslinked A673 lysates, which confirmed the interaction of EWSR1 (n = 3, $p = 0.04$, Student's *t*-test) and RNA Pol II (n = 3, $p > 0.05$, Student's *t*-test) in Ewing sarcoma cells (**Figure 4D**).

EWS-FLI1 is found in a protein granule in cells

We previously used transmission electron microscopy (TEM) to image crosslinked protein particles immunopurified from cell lysates (Thompson et al. 2018). We asked whether this approach could confirm that EWS-FLI1 was present in a large protein body in cells. First, we tested whether crosslinked EWS-FLI1 retained its interactions with EWSR1 and RNA Pol II.

We performed IP assays from HEK293T/17 cells transfected with V5-tagged EWS-FLI1. By ELISA, EWS-FLI1 was found highly enriched in eluates from EWSR1 IP experiments compared with negative protein G bead controls (n = 3, $p = 0.01$, Student's *t*-test, **Figure 5A**). EWS-FLI1 was likewise enriched in RNA Pol II IP experiments compared with negative controls (n = 3, $p = 0.03$, Student's *t*-test, **Figure 5A**). We also found EWSR1 and RNA Pol II to pulldown with an EWS-FLI1 IP (**Supplemental Figure S5A** and **S5B**). We tested whether the ability for EWS-FLI1 to oligomerize might play a role in its ability to bind EWSR1 or RNA Pol II. Replacing the tyrosine residues with serine in the repeated [S/G]Y[S/G] motif of the LC-domain can prevent oligomerization (Kato et al. 2012; Kwon et al. 2013). We transfected in HEK293T/17 cells a V5-tagged EWS-FLI1 construct with 37 tyrosine residues replaced by serine (YS37). Expression for YS37 was comparable to that of wild-type EWS-FLI1 (**Supplemental Figure S5C** and **S5D**). The IP assays for EWSR1 or RNA Pol II failed to recover the YS37 fusion protein (n = 3, $p > 0.05$, Student's *t*-test, **Figure 5B**). The reciprocal IP of YS37 also did not find enrichment of EWSR1 or RNA Pol II (**Supplemental Figure S5E** and **S5F**). This result suggested that the oligomerization found during phase separation may be required for the fusion protein to interact with EWSR1 or RNA Pol II in cells. We also tested whether EWSR1 and RNA Pol II crosslinked and pulled down with the endogenous EWS-

FLI1 protein in A673 cells . In the Ewing sarcoma cell line, EWS-FLI1 also eluted with EWSR1 or RNA Pol II at levels higher than those of negative controls (n = 4, $p < 0.05$, Student's *t*-test, **Figure 5C**).

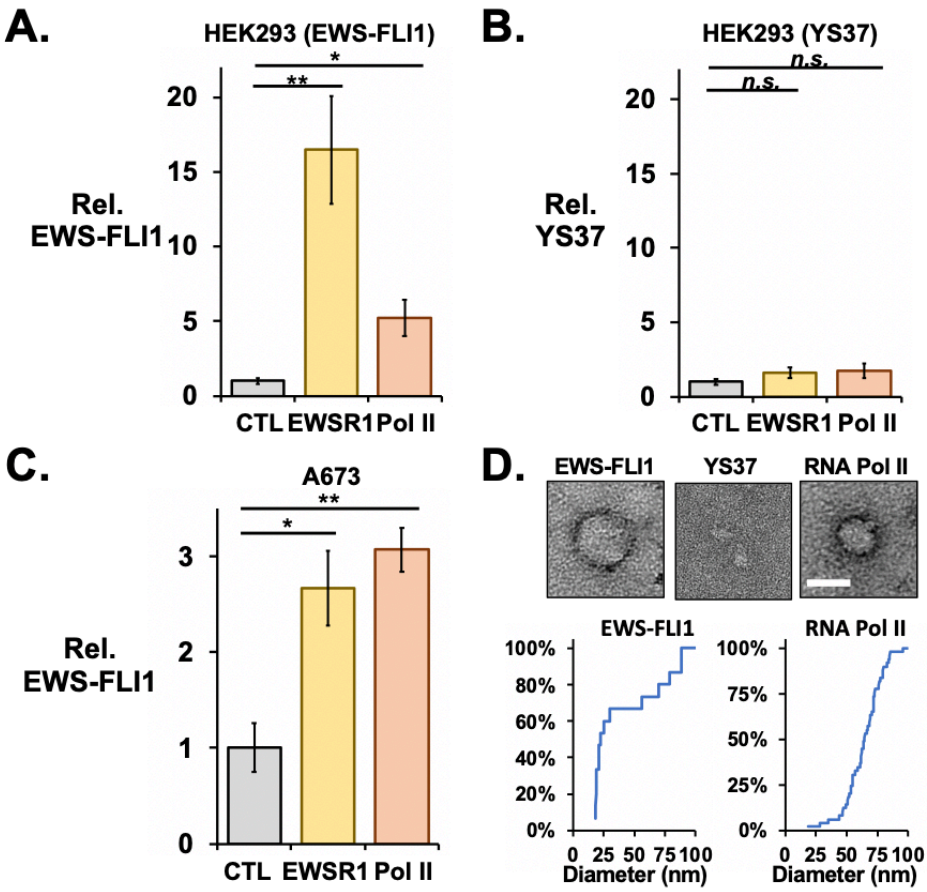

Figure 5. EWS-FLI1 and RNA Pol II coimmunoprecipitate in crosslinked protein granules. Crosslinked IP assays of EWSR1 or RNA Pol II recovered wild-type (**A**) but not a YS37 (**B**) EWS-FLI1 protein when expressed from plasmid in HEK293T/17 cells (n = 3 each). (**C**) Crosslinked IP assays of EWSR1 and RNA Pol II also recovered endogenous EWS-FLI1 from A673 cells (n = 4). All error bars represent standard error about the mean. (**D**) Transmission electron microscopy detected protein particles recovered from crosslinked HEK293T/17 cells by IP of EWS-FLI1 (left) and RNA Pol II (left), but not of YS37 (center). Scale bar inset represents 50 nm. Cumulative plots show diameters for particles imaged in IP samples for EWS-FLI1 (n = 24) or RNA Pol II (n = 77). Student's *t*-test was calculated assuming equal variances: ** $p < 0.01$; * $p < 0.05$; n.s., not significant ($p > 0.05$).

Finally, we investigated whether the IP assays from crosslinked HEK293T/17 lysates recovered granular bodies. We used negative-stained TEM to image particles recovered by IP of RNA Pol II in HEK293T/17 cells, which we had previously reported (Thompson et al. 2018). We observed round particles up to 95 nm in diameter recovered in the RNA Pol II IP samples. RNA Pol II holoenzyme would be expected to appear as particle of 15 to 25 nm. Particles of the size of the polymerase or larger were observed to have an average diameter of 64 ± 15 nm (n = 77, **Figure 5D**). We confirmed that the particles observed were composed of protein by treating samples with proteinase K, which eliminated the round particles observed during TEM (**Supplemental Figure S6**).

We tested whether particles were also observable in EWS-FLI1 IP samples from crosslinked lysates of HEK293T/17 cells that expressed V5-EWS-FLI1. Round particles were observed by TEM to elute from the IP of EWS-FLI1 (**Figure 5D,** middle panels). The particles were found across a broader range of sizes with an average diameter of 42 ± 27 nm (n = 24). To test whether the particles were specific for EWS-FLI1 and to confirm the fusion protein's ability to oligomerize by homotypic interactions, we performed the same IP experiment and TEM imaging using HEK293T/17 cells expressing the YS37 variant of EWS-FLI1. The IP of the YS37 mutant did not reveal any round particles that were visible by TEM (**Figure 5D**). This was consistent with the expectation that YS37 would be incapable of oligomerization or phase separation.

We have found that EWSR1 and EWS-FLI1 regulate many of the same genes and both are required for Ewing sarcoma cells to maintain growth under anchorage-independent conditions. Expression of the fusion protein can cause non-Ewing cells to depend on EWSR1 for colony growth in a soft agar assay, which suggests the fusion protein is responsible for the effect of EWSR1 on cell growth. By confirming that EWS-FLI1 and EWSR1 interact in the affected cells, the ability of the fusion protein to modify EWSR1 activity may be the result of protein–protein interactions. To explore the context for interactions formed by EWS-FLI1 or EWSR1, we showed that EWSR1 inhabits large bodies in cells comparable to those for RNA Pol II. Crosslinked EWS-FLI1 was bound to RNA Pol II and EWSR1, but without its tyrosine residues that are required to form oligomers, it could not bind either protein. We used TEM to observe large protein particles that immunopurified with EWS-FLI1 and appeared similar to those associated with RNA Pol II. Again, the tyrosine residues in the LC domain were required in order to observe the crosslinked particles after immunopurification. This revealed a new property of EWS-FLI1 that the LC domain allows it to assemble into protein particles in the cell . Whereas each protein is found to interact with each other and

incorporate into similar protein particles, our results support the model that EWS-FLI1, EWSR1, and RNA Pol II interact in the nucleus within a protein granule.

DISCUSSION

EWSR1 and EWS-FLI1 each contain the same disordered domain with a capacity for self-oligomerization. Results of this study support a model in which EWS-FLI1 and EWSR1 regulate transcription for hundreds of identical gene targets. EWSR1 and the fusion protein are each required to maintain the signature property of transformation, anchorage-independent cell growth. In addition to these shared functional capacities, these proteins interact physically with each other. EWSR1 is found almost entirely in large particles in the cell, like those containing RNA Pol II. We have also found that EWS-FLI1 and RNA Pol II associate with particles of similar size and appearance , as shown by TEM analysis. This is consistent with the hypothesis that the ability of EWS-FLI1 to self-oligomerize may tie its function in cells to protein granules. The conclusion of this study offers new support to the model that interactions made by EWS-FLI1 occur in the context of a higher-order structure rather than traditional macromolecular complexes (Gorthi et al. 2018; Johnson et al. 2017; Chong et al. 2018).

We found that EWS-FLI1 affected transcript levels for nearly half the genes whose transcripts were also affected by EWSR1. EWS-FLI1 can either increase or reduce transcript levels for affected genes (**Figure 1B**). Several mechanisms may contribute to the ability of EWS-FLI1 to alternate its effects on transcription. EWS-FLI1 has been noted to bind both activator and repressor complexes and its interacting partners may depend on the sites in genomic DNA where the fusion protein binds (Riggi et al. 2014; Boulay et al. 2017; Sankar et al. 2013). The effects of EWSR1 on genes also targeted by the fusion protein are remarkably similar. Our result that hundreds of genes can be affected by both EWS-FLI1 and EWSR1 may be a lower estimate, because EWSR1 concentrations in the cell are quite high (~8 μM) and proteomics studies have indicated levels of endogenous EWS-FLI1 to be much lower (Elzi et al. 2014; Hein et al. 2015; Gierisch et al. 2016). Consequently, siRNA knockdown may more effectively abolish the activity of EWS-FLI1, resulting in effects that were seen for more genes and changes to transcript levels that were generally greater than those found with the EWSR1 knockdown.

In addition to the large number of genes affected by both EWSR1 and EWS-FLI1, the capacity for anchorage-independent growth was affected by both proteins, which extends the functions in common for the fusion and wild-

type proteins to include cellular functions (**Figure 2A**). A role for EWSR1 in this aspect of cell growth is not typical of transformed cells, as we have shown for HEK293T/17 cells (**Figure 2C**). However, expression of EWS-FLI1 from a transfected plasmid was sufficient to reproduce the dependence of cell proliferation on EWSR1 (**Figure 3**). This result is consistent with a hypothesis that EWS-FLI1 can modify EWSR1 function in the cell. We confirmed the interaction between the proteins in transfected HEK293T/17 cells, which offers at least one basis to explain the functional relationship between the proteins (**Supplemental Figure S3B**).

Having seen the potential importance of interactions between EWSR1 and EWS-FLI1, we investigated the characteristics of protein interactions made by EWSR1, RNA Pol II, and EWS-FLI1 in cells. An ordinary protein interaction would be expected to result in a discrete macromolecular complex. Examples of these might range from the dimeric interactions typical of steroid hormone receptors to the 48-mer structure of the 26S proteasome or the RNA Pol II holoenzyme itself. However, EWSR1 and EWS-FLI1 have been shown to oligomerize into higher-order assemblies (Chong et al. 2018; Kwon et al. 2013). Examples of assemblies can include those with distinctive structures, such as actin fibers and nuclear pore complexes (Wu and Fuxreiter 2016). Higher-order assemblies also include a phase separation arising from weak multivalent interactions that yield rounded amorphous shapes reminiscent of a liquid drop in suspension (Lin et al. 2015; Banani et al. 2016; Molliex et al. 2015). As seen for studies with recombinant LC domain proteins, the EWS-FLI1 particles we recovered from cells have the appearance of the liquid-like phase separation of a protein or ribonucleoprotein granule (**Figure 5D**).

FET proteins contain an LC domain that is intimately tied to normal cell processes and disease states. Ewing sarcoma is an example where wild-type and aberrant LC domain proteins exist and interact in the same system. The multivalent interactions driving LC domain assembly form through π-bonds involving tyrosine residues in the repeated [S/G]Y[S/G] motifs (Murray et al. 2017; Lin et al. 2017; Qamar et al. 2018; Wang et al. 2018; Hughes et al. 2018). Tyrosine-rich LC domains are found in many RNA-binding proteins of the hnRNP family, which can allow these proteins to undergo phase separation together through homotypic interactions. We could confirm that the interactions of EWS-FLI1 with EWSR1 or RNA Pol II required these tyrosine residues (**Figure 5B**). The same was true for the assembly of EWS-FLI1 into protein granules that were seen with TEM (**Figure 5D**). This suggests that the protein is functional when it can form higher-order assemblies. Because EWS-FLI1 binding partners are

found in similar protein bodies in the cell, their interactions with each other may be through assembly into a granule together.

The inclusion of fusion proteins driving Ewing sarcoma into granules like those observed for FET proteins and RNA Pol II raises exciting new questions that can be explored in future studies. Do all three FET proteins combine in a single protein granule with the fusion protein? Translocations involving a FET protein are especially powerful driver mutation and a FET protein LC domain is found in nearly half of fusion proteins implicated in sarcomas (Riggi et al. 2007). The high conservation of three distinct genes throughout vertebrates can argue that they have critical but independent functions. However, the mechanisms that can initiate sarcoma development may lie in an area where the functions of the FET proteins overlap. Second, is recruitment of hnRNP proteins and RNA processing machineries common at sites along DNA bound by EWS-FLI1 or other FET-fusion proteins? If true, this would offer at least three possibilities to explore: RNA polymerase can be recruited by RNA processing machinery to initiate transcription of genes; transcription may be suppressed for some genes if the fusion protein directs their RNA processing machinery elsewhere; and, the localization of RNA processing machinery may contribute to reprogramming transcription to promote tumorigenesis. Last, because the fusion protein binds and recruits promiscuous RNA-binding proteins, what RNA transcripts interact with the assemblies and what roles might they serve? One key step in exploring these questions will be to determine whether EWS-FLI1 and other FET-fusion proteins inhabit various nuclear complexes or granules with distinct and independent functions, including those that may not be bound to DNA.

MATERIALS AND METHODS

Cell Culture

Cell lines were obtained from American Type Culture Collection. A673 and SK-N-MC cells were grown in Dulbecco's modified Eagle Medium (DMEM, Thermo Fisher) supplemented with 10% fetal bovine serum (FBS). HEK293T/17 cells were grown in DMEM supplemented with 5% FBS. All cell lines were cultured at 37°C and 5% CO_2.

Plasmid and siRNA Transfections

The siRNAs used were siSCR 5′-GAUGCAGACAUUCAGGAUGUU-3′; siEF 5′-GCUUCUAGUAGUAGCUGCCUU-3′; siEWSR1 5′-CUACUAGAUGCAGAGACCCUU-3′; siE-EF 5′-GACCGCCUAUGCAACUUCUUU-3′. All siRNAs were annealed to its complement strand. The plasmids used, pLV-V5-EWS-FLI1 and pLV-V5-EWS(YS37)-FLI1, were a gift from the M. Rivera lab (Harvard Medical School, Charlestown MA).A673 cells were reverse transfected with siRNA at 5.0×10^5 cells in 6-well dishes using Lipofectamine™ RNAiMAX (Invitrogen, cat. no.13778075) according to manufacturer's instructions. HEK293T/17 and SK-N-MC cells were plated at 4.0×10^5 in 6-well dishes 24 hours before to transfection using the TransIT-X2 reagent (Mirus Bio cat. no. MIR6000) or RNAiMAX. All siRNA transfections were at a final concentration of 50 nM and cells were harvested 48 to 72 hours post-transfection for analysis by western blot. For plasmid transfections, HEK293T/17 cells were transfected at 80% confluency. Cells were transfected using TransIT-X2 reagent following manufacturer's instructions. Cells were harvested 48 to 96 hours post-transfection.

Western Blot Analysis

Protein lysate concentrations were quantified using the bicinchoninic (BCA) protein assay (ThermoFisher, cat. no. 23227). Protein samples of 5 to 10 μg were loaded onto 7.5% SDS-PAGE gels. Blots were transferred at 500 mA, blocked in 5% nonfat dried milk in Tris-buffered saline-Tween(TBS-T), and incubated overnight with primary antibody at 4°C. Blots were washed in TBS-T, incubated in secondary antibody for 1 hour at room temperature, washed again in TBS-T, and imaged after the addition of SuperSignal™ West Pico PLUS Chemiluminescent substrate (ThermoFisher, Cat. #34578). Antibodies used in western blots were anti-EWSR1 (Santa Cruz Biotechnology, cat. no. 398318), anti-FLI1 (Abcam, cat. no. 15289), anti-RNA Pol II (clone CTD4H8, EMD Millipore, cat. no. 05-623), anti-RNA Pol II CTD phospho S5 (Abcam, cat. no. 5131), and anti-V5 (Abcam, cat. no. 27671); secondary antibodies used were donkey anti-mouse IgG horseradish peroxidase (HRP) (Jackson ImmunoResearch, cat. no. 715-035-15) and donkey anti-rabbit IgG HRP (Jackson ImmunoResearch, cat. no. 711-035-152).

RNA Sequencing

A673 cells were transfected with 50 nM siRNA as described above. Cells were collected 72 hours post-transfection and total RNA was extracted using TRIzol reagent (ThermoFisher, cat. no. 15596026). RNA (1 μg) was prepared for sequencing using NEBNext Poly(A) mRNA Magnetic Isolation Module (New England Biolabs, cat. no. E7490) to generate sequencing libraries according to the manufacturer's instructions.

Soft Agar Colony Formation Assay

A673, SK-N-MC, and HEK293T/17 cells transfected with 50 nM siRNA were harvested at 24 hours post-transfection. HEK293T/17 cells transfected with 50 nM siRNA and 2 μg of plasmid DNA were harvested 24 hours post-transfection. A673 and SK-N-MC cells were seeded at density of 1.0×10^5 cells. Cells were resuspended in 0.35% agarose in growth medium and plated onto a bed of solidified 0.6% agarose in growth media. HEK293T/17 cells were seeded at a density of 20k to 30k cells. Cells were resuspended in 0.4% agarose in growth medium onto a bed of solidified 0.6% agarose in growth media. A673 and SK-N-MC cells were grown at 37°C and 5% CO_2 for 3 to 4 weeks, imaged, and then colonies were counted using ImageJ software. HEK293T/17 cells were grown at 37°C and 5% CO_2 for 1 to 2 weeks, imaged, and then colonies were counted. Colonies with stained with 0.05% methylene blue.

Cell Growth Assay

A673 cells were reverse transfected at a density of 4.0×10^5 cells in 6-well dishes. Cells were collected by trypsinization and counted on a hemocytometer at 24, 48, 72, and 96-hour time points post-transfection.

Co-Immunoprecipitation Assay

Co-immunoprecipitation assays (co-IP) were performed with cells. Cells were harvested from 6-well plates and lysed in co-IP lysis/wash buffer (25 mM Tris-HCl pH 7.4, 200 mM NaCl, 1 mM EDTA, 0.5% NP40, 5% glycerol). Protein A/G agarose beads (EMD Millipore, cat. no. IP05) were incubated with primary antibody for 2 hours at 4°C before addition to cell lysate. Lysate was incubated with beads-antibody complex overnight with rotation at 4°C. Beads were washed 5 times in co-IP lysis/wash buffer, resuspended in Novex NuPage™ Sample Loading Buffer

(Fisher Scientific, cat. no. np0008) with 5 mM dithiothreitol (DTT) and boiled for 5 minutes at 95°C. Beads were then centrifuged at 8000 rpm and eluted protein removed with the supernatant and detected by western blot.

For crosslinked co-IP assays, cells were harvested from confluent 150-mm dishes. Cells were crosslinked in 1% formaldehyde for 15 minutes and then quenched in 125 mM glycine. Cells were washed in phosphate-buffered saline (PBS) and lysed in Buffer B (1% SDS, 10 mM EDTA, 50 mM Tris-HCl pH 8.0) supplemented with protease inhibitors. Lysate was sonicated using a Bioruptor Pico (Diagenode) for 30 minutes and then centrifuged at maximum speed (20000×*g*) for 30 minutes at 4°C. Crosslinked lysate was diluted 10-fold in IP lysis buffer (0.01% SDS, 1.1% Triton-X, 1.2 mM EDTA, 16.7 mM Tris-HCl pH 8.0, 167 mM NaCl) treated with protease inhibitors (Sigma-Aldrich, cat. no. P8340) and benzonase (Millipore-Sigma, cat. no. 70746). Lysate was then incubated with rotation overnight with primary antibody at 4°C. Antibody-bound complexes were immunoprecipitated with Novex DYNAL Dynabeads Protein G (Invitrogen, cat. no. 10-003-D) or protein A/G agarose beads (EMD Millipore, cat. no. IP05) for 2 hours at room temperature. Beads were washed 5 times using IP lysis buffer and eluted in 3.6 M $MgCl_2$ and 20 mM 2-(*N*-morpholino)ethanesulfonic acid (MES, pH 6.5) for 30 minutes with agitation. IP samples were then assayed for proteins by ELISA.

Size Exclusion Chromatography

The protocol for SEC of crosslinked lysates has been previously described (Thompson et al. 2018). For crosslinked lysates, cells were harvested from confluent 150-mm dishes. Cells were crosslinked in 1% formaldehyde for 15 minutes and then quenched in 125 mM glycine. Cells were harvested by scraping, washed in PBS, and resuspended in 5 to 10 volumes of Buffer C (400 mM NaCl, 20 mM HEPES pH 7.9, 5% glycerol, 0.75 mM $MgCl_2$, and 6 M urea). Lysates were sonicated using a Bioruptor Pico (Diagenode) for 30 minutes at 4°C, followed by centrifugation at maximum speed (20000×*g*) for 30 minutes at 4°C , then filtered through a Costar Spin-X 0.45 µm filter (VWR, cat. no. 8163). Lysate (1 to 2 mg) was injected onto the column. SEC was performed using a Sepharose CL-2B 10/300 column (Sigma-Aldrich, cat. no. CL2B300, 100 mL) injected with lysates from HEK293T/17 or A673 cells. Columns were run in Buffer B (100 mM NaCl, 20 mM HEPES pH 7.9, 0.2 mM EDTA, 5% glycerol, 6 M urea, and 0.5 mM DTT).

ELISA

ELISAs were performed in 96-well Greiner LUMITRAC-600 white plates (VWR, cat. no. 82050-724). ELISAs were performed as indirect ELISAs, in which protein samples from SEC or crosslinked IP assays were incubated in plates overnight at 4°C. Afterward, plates were washed 3 times in TBS-T, blocked for 2 hours at room temperature in 5% nonfat dried milk in TBS-T, washed 4 times in TBS-T and then incubated with primary antibody overnight at 4°C. After incubation with primary antibody, plates were washed 4 times in TBS-T and incubated with secondary antibody, goat anti-mouse IgG HRP (ThermoFisher cat. no. 31432) or goat anti-rabbit IgG HRP (ThermoFisher, Cat. #31462) for 1 hour at room temperature. Finally, plates were washed 4 times with TBST and proteins were detected by addition of SuperSignal™ ELISA Femto substrate (ThermoFisher cat. no. PI37074). Luminescence was read using a BMG POLARstar Omega plate reader or Biotek Neo2 microplate reader.

Transmission Electron Microscopy

Carbon Film 300 Mesh Copper grids (Electron Microscopy Sciences, cat. no. CF300-CU) were charged at 15 mA for 30 seconds. Crosslinked immunoprecipitation samples were spotted onto charged grids and stained with 0.75% uranyl formate. For proteinase K-treated samples, the samples were treated with 5 μg of proteinase K and incubated for 30 minutes at 37°C before being spotted onto grids and stained with 0.75% uranyl formate. Images were collected from a FEI Tecnai Spirit 120S or FEI Tecnai F20 transmission electron microscope.

Corresponding Author

Correspondence should be addressed to Jacob C. Schwartz at jcschwartz@arizona.edu.

Author Contributions

N.S.A. designed and performed experiments, analyzed data, and interpreted results. L.M.H. contributed the design of siRNAs and performed the screening and optimization siRNA knockdown using real-time PCR and western assays. L.M.H. also contributed to multiple procedures that involved the use of recombinant DNA. N.S.A. wrote the first draft of the manuscript. N.S.A. and J.C.S. collaborated to write subsequent drafts. All authors have approved to the final version of the manuscript.

Funding Sources and Acknowledgements

This work was supported by funding from the National Institutes of Health (R21CA238499) and the American Cancer Society (RSG-18-237-01-DMC) to J.C.S. Additional support was provided by National Institute of General Medicine (T32-GM008659) training grant awarded to N.S.A. Next-generation sequencing was performed by the University of Arizona Genetics Core, http://uagc.arizona.edu. Transmission election microscopy was performed with the Eyring Materials Center at Arizona State University, supported in part by NNCI-ECCS-1542160. Transmission Electron Microscopy was also performed through the University of Arizona Office of Research, Innovation, & Impact Imaging Cores. Research reported in this publication was also supported by the Office of the Director, National Institutes of Health of the National Institutes of Health, under award number S10OD013237.

REFERENCES

Bailly RA, Bosselut R, Zucman J, Cormier F, Delattre O, Roussel M, Thomas G, Ghysdael J. 1994. DNA-binding and transcriptional activation properties of the EWS-FLI-1 fusion protein resulting from the t(11;22) translocation in Ewing sarcoma. *Mol Cell Biol* **14**: 3230–3241.

Banani SF, Rice AM, Peeples WB, Lin Y, Jain S, Parker R, Rosen MK. 2016. Compositional Control of Phase-Separated Cellular Bodies. *Cell* **166**: 651–663.

Blechingberg J, Luo Y, Bolund L, Damgaard CK, Nielsen AL. 2012. Gene Expression Responses to FUS, EWS, and TAF15 Reduction and Stress Granule Sequestration Analyses Identifies FET-Protein Non-Redundant Functions. *PLoS One* **7**.

Boeynaems S, Alberti S, Fawzi NL, Mittag T, Polymenidou M, Rousseau F, Schymkowitz J, Shorter J, Wolozin B, Van Den Bosch L, et al. 2018. Protein Phase Separation: A New Phase in Cell Biology. *Trends Cell Biol* **28**: 420–435.

Boulay G, Sandoval GJ, Riggi N, Iyer S, Buisson R, Naigles B, Awad ME, Rengarajan S, Volorio A, McBride MJ, et al. 2017. Cancer-Specific Retargeting of BAF Complexes by a Prion-like Domain. *Cell* **171**: 163-178.e19.

Chaturvedi A, Hoffman LM, Welm AL, Lessnick SL, Beckerle MC. 2012. The EWS/FLI Oncogene Drives Changes in Cellular Morphology, Adhesion, and Migration in Ewing Sarcoma. *Genes and Cancer* **3**: 102–116.

Chi B, O'Connell JD, Yamazaki T, Gangopadhyay J, Gygi SP, Reed R. 2018. Interactome analyses revealed that the U1 snRNP machinery overlaps extensively with the RNAP II machinery and contains multiple ALS/SMA-causative proteins. *Sci Rep* **8**: 8755. https://www.ncbi.nlm.nih.gov/pubmed/29884807.

Chong S, Dugast-Darzacq C, Liu Z, Dong P, Dailey GM, Cattoglio C, Heckert A, Banala S, Lavis L, Darzacq X, et al. 2018. Imaging dynamic and selective low-complexity domain interactions that

control gene transcription. *Science (80-)* **361**.

Delattre O, Zucman J, Plougastel B, Desmaze C, Melot T, Peter M, Kovar H, Joubert I, De Jong P, Rouleau G, et al. 1992. Gene fusion with an ETS DNA-binding domain caused by chromosome translocation in human tumours. *Nature* **359**: 162–165.

Elzi DJ, Song M, Hakala K, Weintraub ST, Shiio Y. 2014. Proteomic analysis of the EWS-Fli-1 interactome reveals the role of the lysosome in EWS-Fli-1 turnover. *J Proteome Res* **13**: 3783–3791.

Embree LJ, Azuma M, Hickstein DD. 2009. Ewing sarcoma fusion protein EWSR1/FLI1 interacts with EWSR1 leading to mitotic defects in zebrafish embryos and human cell lines. *Cancer Res* **69**: 4363–4371.

Gangwal K, Sankar S, Hollenhorst PC, Kinsey M, Haroldsen SC, Shah AA, Boucher KM, Watkins WS, Jorde LB, Graves BJ, et al. 2008. Microsatellites as EWS/FLI response elements in Ewing's sarcoma. *Proc Natl Acad Sci U S A* **105**: 10149–10154.

Gierisch ME, Pfistner F, Lopez-Garcia LA, Harder L, Schäfer BW, Niggli FK. 2016. Proteasomal degradation of the EWS-FLI1 fusion protein is regulated by a single lysine residue. *J Biol Chem* **291**: 26922–26933.

Gorthi A, Romero JC, Loranc E, Cao L, Lawrence LA, Goodale E, Iniguez AB, Bernard X, Masamsetti VP, Roston S, et al. 2018. EWS-FLI1 increases transcription to cause R-Loops and block BRCA1 repair in Ewing sarcoma. *Nature* **555**: 387–391.

Grünewald TGP, Cidre-Aranaz F, Surdez D, Tomazou EM, De Álava E, Kovar H, Sorensen PH, Delattre O, Dirksen U. 2018. Ewing sarcoma. *Nat Rev Dis Prim* **4**.

Hein MY, Hubner NC, Poser I, Cox J, Nagaraj N, Toyoda Y, Gak IA, Weisswange I, Mansfeld J, Buchholz F, et al. 2015. A Human Interactome in Three Quantitative Dimensions Organized by Stoichiometries and Abundances. *Cell* **163**: 712–723.

Hoell JI, Larsson E, Runge S, Nusbaum JD, Duggimpudi S, Farazi TA, Hafner M, Borkhardt A, Sander

C, Tuschl T. 2011. RNA targets of wild-type and mutant FET family proteins. *Nat Struct Mol Biol* **18**: 1428–1431.

Hughes MP, Sawaya MR, Boyer DR, Goldschmidt L, Rodriguez JA, Cascio D, Chong L, Gonen T, Eisenberg DS. 2018. Atomic structures of low-complexity protein segments reveal kinked b sheets that assemble networks. *Science (80-)* **359**: 698–701.

Jain S, Wheeler JR, Walters RW, Agrawal A, Barsic A, Parker R. 2016. ATPase-Modulated Stress Granules Contain a Diverse Proteome and Substructure. *Cell* **164**: 487–498.

Johnson KM, Mahler NR, Saund RS, Theisen ER, Taslim C, Callender NW, Crow JC, Miller KR, Lessnick SL. 2017. Role for the EWS domain of EWS/FLI in binding GGAA-microsatellites required for Ewing sarcoma anchorage independent growth. *Proc Natl Acad Sci* **114**: 9870–9875.

Kato M, Han TW, Xie S, Shi K, Du X, Wu LC, Mirzaei H, Goldsmith EJ, Longgood J, Pei J, et al. 2012. Cell-free formation of RNA granules: Low complexity sequence domains form dynamic fibers within hydrogels. *Cell* **149**: 753–767.

Kato M, McKnight SL. 2018. A Solid-State Conceptualization of Information Transfer from Gene to Message to Protein. *Annu Rev Biochem* **87**: 351–390.

Kovar H, Aryee DNT, Jug G, Henöckl C, Schemper M, Delattre O, Thomas G, Gadner H. 1996. EWS/FLI-1 antagonists induce growth inhibition of Ewing tumor cells in vitro. *Cell Growth Differ* **7**: 429–437.

Kwon I, Kato M, Xiang S, Wu L, Theodoropoulos P, Mirzaei H, Han T, Xie S, Corden JL, McKnight SL. 2013. XPhosphorylation-regulated binding of RNA polymerase II to fibrous polymers of low-complexity domains. *Cell* **155**: 1049.

Lin Y, Currie SL, Rosen MK. 2017. Intrinsically disordered sequences enable modulation of protein phase separation through distributed tyrosine motifs. *J Biol Chem* **292**: 19110–19120.

Lin Y, Protter DSW, Rosen MK, Parker R. 2015. Formation and Maturation of Phase-Separated Liquid Droplets by RNA-Binding Proteins. *Mol Cell* **60**: 208–219.

Luo Y, Blechingberg J, Fernandes AM, Li S, Fryland T, Børglum AD, Bolund L, Nielsen AL. 2015. EWS and FUS bind a subset of transcribed genes encoding proteins enriched in RNA regulatory functions. *BMC Genomics* **16**: 1–17.

Masuda A, Takeda JI, Okuno T, Okamoto T, Ohkawara B, Ito M, Ishigaki S, Sobue G, Ohno K. 2015. Position-specific binding of FUS to nascent RNA regulates mRNA length. *Genes Dev* **29**: 1045–1057.

Molliex A, Temirov J, Lee J, Coughlin M, Kanagaraj AP, Kim HJ, Mittag T, Taylor JP. 2015. Phase separation by low complexity domains promotes stress granule assembly and drives pathological fibrillization. *Cell* **163**: 123–133. https://www.ncbi.nlm.nih.gov/pubmed/26406374.

Moore MJ, Proudfoot NJ. 2009. Pre-mRNA Processing Reaches Back toTranscription and Ahead to Translation. *Cell* **136**: 688–700.

Murray DT, Kato M, Lin Y, Thurber KR, Hung I, McKnight SL, Tycko R. 2017. Structure of FUS Protein Fibrils and Its Relevance to Self-Assembly and Phase Separation of Low-Complexity Domains. *Cell* **171**: 615-627.e16.

Ozdilek BA, Thompson VF, Ahmed NS, White CI, Batey RT, Schwartz JC. 2017. Intrinsically disordered RGG/RG domains mediate degenerate specificity in RNA binding. *Nucleic Acids Res* **45**: 7984–7996.

Paronetto MP, Miñana B, Valcárcel J. 2011. The Ewing Sarcoma Protein Regulates DNA Damage-Induced Alternative Splicing. *Mol Cell* **43**: 353–368.

Qamar S, Wang GZ, Randle SJ, Ruggeri FS, Varela JA, Lin JQ, Phillips EC, Miyashita A, Williams D, Ströhl F, et al. 2018. FUS Phase Separation Is Modulated by a Molecular Chaperone and Methylation of Arginine Cation-π Interactions. *Cell* **173**: 720-734.e15.

Riggi N, Cironi L, Provero P, Suvà ML, Kaloulis K, Garcia-Echeverria C, Hoffmann F, Trumpp A, Stamenkovic I. 2005. Development of Ewing's sarcoma from primary bone marrow-derived mesenchymal progenitor cells. *Cancer Res* **65**: 11459–11468.

Riggi N, Cironi L, Suvà M-L, Stamenkovic I. 2007. Sarcomas: genetics, signalling, and cellular origins. Part 1: The fellowship of TET. *J Pathol* **213**: 4–20.

Riggi N, Knoechel B, Gillespie SM, Rheinbay E, Boulay G, Suvà ML, Rossetti NE, Boonseng WE, Oksuz O, Cook EB, et al. 2014. EWS-FLI1Utilizes Divergent Chromatin Remodeling Mechanisms to Directly Activate or Repress Enhancer Elements in Ewing Sarcoma. *Cancer Cell* **26**: 668–681.

Riggi N, Suvà ML, Suvà D, Cironi L, Provero P, Tercier S, Joseph JM, Stehle JC, Baumer K, Kindler V, et al. 2008. EWS-FLI-1 expression triggers a ewing's sarcoma initiation program in primary human mesenchymal stem cells. *Cancer Res* **68**: 2176–2185.

Rogelj B, Easton LE, Bogu GK, Stanton LW, Rot G, Curk T, Zupan B, Sugimoto Y, Modic M, Haberman N, et al. 2012. Widespread binding of FUS along nascent RNA regulates alternative splicing in the brain. *Sci Rep* **2**: 1–10.

Sankar S, Bell R, Stephens B, Zhuo R, Sharma S, Bearss DJ, Lessnick SL. 2013. Mechanism and relevance of EWS/FLI-mediated transcriptional repression in Ewing sarcoma. *Oncogene* **32**: 5089–5100.

Schwartz JC, Cech TR, Parker RR. 2015. Biochemical Properties and Biological Functions of FET Proteins. *Annu Rev Biochem* **84**: 355–379.

Schwartz JC, Ebmeier CC, Podell ER, Heimiller J, Taatjes DJ, Cech TR. 2012. FUS binds the CTD of RNA polymerase II and regulates its phosphorylation at Ser2. *Genes Dev* **26**: 2690–2695.

Schwartz JC, Wang X, Podell ER, Cech TR. 2013. RNA Seeds Higher-Order Assembly of FUS Protein. *Cell Rep* **5**: 918–925.

Selvanathan SP, Graham GT, Grego AR, Baker TM, Hogg JR, Simpson M, Batish M, Crompton B, Stegmaier K, Tomazou EM, et al. 2019. EWS–FLI1 modulated alternative splicing of ARID1A reveals novel oncogenic function through the BAF complex. *Nucleic Acids Res* **47**: 9619–9636.

Smith R, Owen LA, Trem DJ, Wong JS, Whangbo JS, Golub TR, Lessnick SL. 2006. Expression profiling of EWS/FLI identifies NKX2.2 as a critical target gene in Ewing's sarcoma. *Cancer Cell*

9: 405–416.

Spahn L, Siligan C, Bachmaier R, Schmid JA, Aryee DNT, Kovar H. 2003. Homotypic and heterotypic interactions of EWS, FLI1 and their oncogenic fusion protein. *Oncogene* **22**: 6819–6829.

Tan AY, Manley JL. 2009. The TET family of proteins: Functions and roles in disease. *J Mol Cell Biol* **1**: 82–92.

Tanaka K, Iwakuma T, Harimaya K, Sato H, Iwamoto Y. 1997. EWS-Fli1 antisense oligodeoxynucleotide inhibits proliferation of human Ewing's sarcoma and primitive neuroectodermal tumor cells. *J Clin Invest* **99**: 239–247.

Thompson VF, Victor RA, Morera AA, Moinpour M, Liu MN, Kisiel CC, Pickrel K, Springhower CE, Schwartz JC. 2018. Transcription-Dependent Formation of Nuclear Granules Containing FUS and RNA Pol II. *Biochemistry* **57**: 7021–7032.

Wang J, Choi JM, Holehouse AS, Lee HO, Zhang X, Jahnel M, Maharana S, Lemaitre R, Pozniakovsky A, Drechsel D, et al. 2018. A Molecular Grammar Governing the Driving Forces for Phase Separation of Prion-like RNA Binding Proteins. *Cell* **174**: 688-699.e16.

West JA, Mito M, Kurosaka S, Takumi T, Tanegashima C, Chujo T, Yanaka K, Kingston RE, Hirose T, Bond C, et al. 2016. Structural, super-resolution microscopy analysis of paraspeckle nuclear body organization. *J Cell Biol* **214**: 817–830.

Wu H, Fuxreiter M. 2016. The Structure and Dynamics of Higher-Order Assemblies: Amyloids, Signalosomes, and Granules. *Cell* **165**: 1055–1066.

Yang L, Chansky HA, Hickstein DD. 2000. EWS·Fli-1 fusion protein interacts with hyperphosphorylated RNA polymerase II and interferes with serine-arginine protein-mediated RNA splicing. *J Biol Chem* **275**: 37612–37618.

FIGURE LEGENDS

Figure 1. A large number of transcripts had similar responses after a loss of EWS-FLI1 or EWSR1 in Ewing sarcoma. (**A**) Schematic (*top*) shows locations in *EWSR1* or *EWS-FLI1* mRNA targeted by siRNA. Western blots show the reduction in protein levels in A673 cells treated with siRNA targeting EWS-FLI1 (siEF), EWSR1 (siEWSR1) or both (siE-EF). (**B**) A comparison of cells treated with siEF or siEWSR1 revealed a similar increase or decrease in abundance by >1.8-fold for 485 transcripts (green) and in the opposite directions for 54 transcripts (yellow). The number of transcripts changed >1.8-fold are indicated in each quartile.

Figure 2. Loss of EWSR1 inhibits anchorage-independent growth in Ewing sarcoma cells. (**A**) Soft agar assays were performed for A673 cells treated with siSCR, siEF, or siEWSR1. (**B**) Averaged colony numbers in A673 cells were quantified relative to siSCR treatments (n = 3). (**C**) Soft agar assays were performed for HEK293T/17 cells treated with siSCR, siEF, or siEWSR1. (**D**) Averaged colony numbers for HEK293T/17 cells were quantified relative to siSCR treatments (n = 4). Error bars represent standard deviation about the mean. Student's *t*-test was calculated assuming equal variances: ** $p < 0.01$; * $p < 0.05$; n.s., not significant ($p > 0.05$).

Figure 3. Expression of EWS-FLI1 in HEK293T/17 cells recapitulates loss of EWSR1 phenotype. (**A**) Soft agar assays were used to assess anchorage-independent growth of HEK293T/17 cells co-transfected with V5-EWS-FLI1 and either siEWSR1 or siSCR (n = 6). (**B**) The average reduction in colony number for siEWSR1-treated cells was quantified relative to that of siSCR. Error bars represent standard deviation about the mean. Student's *t*-test was calculated for assuming equal variances: *** $p < 0.001$.

Figure 4. EWSR1 and RNA Pol II are assembled in large protein granules. (**A**) Protein eluting from size-exclusion chromatography (SEC) of HEK293T/17 cell lysates was assessed by UV absorbance (top). ELISAs were used to measure RNA Pol II and EWSR1 elution from SEC (n = 3). Dashed lines represent standard error. (**B**) The diagram compares protocols for immunoprecipitation (IP) from cells. Non-crosslinked IP assays preferentially enrich macromolecular complexes. Crosslinked IP assays are capable of recovering weak protein interactions in cell granules. Assays performed used antibodies specific for EWSR1 or CTD phosphorylated at position Ser5 (S5P).

(**C**) ELISAs detected EWSR1 eluted from crosslinked IP assays of S5P in HEK293T/17 cells, and S5P was detected for crosslinked IP of EWSR1 (n = 3). (**D**) In crosslinked IP assays from A673 cells, ELISAs also detected EWSR1 eluted with S5P, and S5P was detected for crosslinked IP of EWSR1 (n = 3). AU = absorbance units. RLU = relative luminescence units. Student's *t*-test was calculated assuming equal variances: ** $p < 0.01$; * $p < 0.05$; n.s., not significant ($p > 0.05$).

Figure 5. EWS-FLI1 and RNA Pol II coimmunoprecipitate in crosslinked protein granules. Crosslinked IP assays of EWSR1 or RNA Pol II recovered wild-type (**A**) but not a YS37 (**B**) EWS-FLI1 protein when expressed from plasmid in HEK293T/17 cells (n = 3 each). (**C**) Crosslinked IP assays of EWSR1 and RNA Pol II also recovered endogenous EWS-FLI1 from A673 cells (n = 4). All error bars represent standard error about the mean. (**D**) Transmission electron microscopy detected protein particles recovered from crosslinked HEK293T/17 cells by IP of EWS-FLI1 (left) and RNA Pol II (left), but not of YS37 (center). Scale bar inset represents 50 nm. Cumulative plots show diameters for particles imaged in IP samples for EWS-FLI1 (n = 24) or RNA Pol II (n = 77). Student's *t*-test was calculated assuming equal variances: ** $p < 0.01$; * $p < 0.05$; n.s., not significant ($p > 0.05$).